

Self-consistent optimization of the z -Expansion for B meson decays

Daniel Simons¹, Erik Gustafson², and Yannick Meurice¹

¹*Department of Physics and Astronomy,*

The University of Iowa

Iowa City, IA 52242, USA and

²*Fermilab, Batavia, IL 60510, USA*

(Dated: May 12, 2023)

Abstract

We discuss the self-consistency imposed by the analyticity of regular parts of form factors, appearing in the z -expansion for semileptonic B -meson decays, when fitted in different kinematic regions. Relying on the uniqueness of functions defined by analytic continuation, we propose four metrics which measure the departure from the ideal analytic self-consistency. We illustrate the process using Belle data for $B \rightarrow D\ell\nu_\ell$. For this specific example, the metrics provide consistent indications that some choices (order of truncation, BGL or BCL) made in the form of the z -expansion can be optimized. However, other choices (z -origin, location of isolated poles and threshold constraints) appear to have very little effect on these metrics. We briefly discuss the implication for optimization of the z -expansion for nucleon form factors relevant for neutrino oscillation experiments.

I. INTRODUCTION

Experimental differential decay rates for exclusive semileptonic decays of B -mesons [1–9], combined with ab-initio lattice QCD calculations of the hadronic form factors [10–22, 24] provide reliable numerical estimations of the CKM matrix elements $|V_{ub}|$ and $|V_{cb}|$. Accurate lattice calculations are only possible for a large enough invariant square of the 4-momentum of the leptons, denoted q^2 , or more specifically when the recoil energy of the final state meson is significantly smaller than the inverse lattice spacing. In order to predict the shape of the differential decay rate over the entire kinematic range from reliable lattice results in the high q^2 region, an analytic continuation method developed in the context of Kaon decays [25, 26] has been adapted for B -meson decays by Boyd, Grinstein and Lebed (BGL) [27] and Bourrely, Caprini and Lellouch (BCL) [28]. The method is often called the z -expansion. The basic idea is to map the branch cut in the complex q^2 plane onto the boundary of the unit disk in z with the rest of the cut complex q^2 plane being mapped into the interior of the disk. The goal is to find parameterizations of the form factors for specific processes where the effects of thresholds and isolated poles can to some extent be separated from a smooth behavior in the kinematic range. Ideally, after the mapping, the kinematic range becomes a small interval near the origin and a few terms in the Taylor expansion provide reliable results. General strategies for combining the lattice and experimental data are discussed in Ref. [11].

The extrapolation of lattice results with computationally accessible q^2 to the full kinematic range relevant for experimental analysis has been performed for various decay modes and by various collaborations [10–22, 24]. Specific choices will be reviewed below. In general, the agreement with the overall shape of the experimental differential decay rate provides a strong guidance to select reasonable procedures. If one assumes the standard model is correct then an ab-initio calculation in the full kinematic range should reproduce the shape of the experimental data. Under this assumption, the only unknown quantity is V_{cb} , a Cabibbo-Kobayashi-Maskawa matrix element. The z -expansion being a compact and model-independent method is very important to summarize the experimental results, especially as it does not depend on the binning procedure. Recent experiments provide fits of their data using the z -expansion. This amounts to continuous functions that allow comparisons among

experiments with different binnings. For semileptonic decays of B -mesons involving tree-level virtual W^\pm bosons, the form factor can be expressed in term of *analytic* functions in the entire kinematic interval. An important implication is that a (perfect) knowledge of the analytic function in any open set in the complex q^2 plane *uniquely* determines the function in the whole interval provided that no singularities or cuts prevent the analytical continuation [29].

In this article, we discuss the self-consistency imposed by analyticity on regular parts of form factors when fitted in different kinematic regions. In Sec. II, we review the BGL and BCL parameterizations. In Sec. III, we consider existing goodness of fit measures (χ^2 and AIC) and define four dimensionless metrics which measure the departure from ideal analytic self-consistency. These metrics are “cost functions” for which a large value indicate an inconsistent parameterization conflicting with the assumed analyticity as defined mathematically in [29]. We illustrate the idea by calculating these four metrics for $B \rightarrow D\ell\nu_\ell$ using partial decays widths provided by the Belle collaboration [6]. The numerical results are analyzed in Sec. IV where we discuss the possibility of discriminating among a certain number of choices (order of truncation, BGL or BCL, z -origin and threshold constraints) made in the z -expansion. The results are summarized in the conclusions where we also comment on new methods of determining the order of truncation of the z -expansion [23, 24]. We also briefly possible applications for optimization of lattice nucleon form factors reviewed in [30] and relevant for neutrino experiments such as DUNE.

II. BGL AND BCL PARAMETERIZATIONS

In the following, we focus on different parameterizations of the form factor that describe the decays $B^0 \rightarrow D^-\ell^+\nu_\ell$ and $B^+ \rightarrow D^0\ell^+\nu_\ell$, with $\ell = \{e, \mu\}$. In the isospin limit, these processes can be described by a differential decay rate that depends on the hadronic recoil variable $w \equiv (m_B^2 + m_D^2 - q^2)/(2m_B m_D)$ [6],

$$\frac{d\Gamma}{dw} = K(w^2 - 1)^{3/2} f_+(w)^2, \quad (1)$$

with

$$K = \frac{G_F^2 m_D^3}{48\pi^3} |V_{cb}|^2 (m_B + m_D)^2 \frac{4r}{(1+r)^2} \eta_{EW}^2, \quad (2)$$

Where G_F is the Fermi coupling constant, m_B and m_D are the masses of the B and D mesons respectively, $r = m_D/m_B$, and η_{EW} represents the electroweak corrections.

The two parameterizations of the vector form factor $f_+(w)$ that we investigate are the BGL and BCL parameterizations. Both parameterizations use the z -expansion which takes the real kinematic range and embeds it into a complex domain, where the process of analytical continuation defines a unique regular (analytic and single-valued) function. The mapping variable is $z(q^2, t_0)$, where:

$$z(q^2, t_0) = \frac{\sqrt{t_+ - q^2} - \sqrt{t_+ - t_0}}{\sqrt{t_+ - q^2} + \sqrt{t_+ - t_0}}, \quad (3)$$

q^2 is the momentum transfer, $q^2 = m_B^2 + m_D^2 - 2wm_Bm_D$, and $t_+ = (m_B + m_D)^2$. This change of coordinates maps the cut complex q^2 plane onto the unit disk. At threshold, $q^2 = t_+$ and $z = -1$. The cut is mapped into the boundary of the disk. The variable t_0 determines where the z -expansion is centered about. We consider two t_0 values $t_0 = t_{opt} = (m_B + m_D)(\sqrt{m_B} - \sqrt{m_D})^2$ and $t_0 = t_- = (m_B - m_D)^2$. The choice of t_0 should not appreciably affect the z -expansion fit results, but it can be used to adjust the systematic uncertainties. Following the original authors, $t_0 = t_{opt}$ is used with BCL [28] and $t_0 = t_-$ is used with BGL [27]. The choice $t_0 = t_{opt}$ puts z in the range $z \in [-0.0323, 0.0323]$, and the choice $t_0 = t_-$ puts z in the range $z \in [0.0, 0.0646]$.

We define the BGL parameterization as $f_{+,BGL}$, with the explicit form used for a lattice calculation [17] and the analysis of the Belle data [6], both for $B \rightarrow D\ell\nu_\ell$.

$$f_{+,BGL}(z) \equiv \frac{1}{\phi_+(z)} \sum_{n=0}^N a_{+,n} z^n, \quad (4)$$

with

$$\phi_+(z) = 1.1213(1+z)^2(1-z)^{1/2}[(1+r)(1-z) + 2\sqrt{r}(1+z)]^{-5}. \quad (5)$$

The outer function, $\phi_+(z)$, is to some extent arbitrary but must be analytic and non-zero

for $|z| < 1$ in order to enforce the unitarity condition on $a_{+,n}$ [6, 27]. We then define the BCL parameterization as $f_{+,BCL}$, with the explicit form used for a lattice calculation [13] $B \rightarrow \pi \ell \nu_\ell$ but with $m_{B^*}^2$ replaced by $m_{B_c^*}^2$.

$$f_{+,BCL}(z) \equiv \frac{1}{1 - q^2(z)/m_{B_c^*}^2} \sum_{k=0}^{K-1} b_{+,k} [z^k - (-1)^{k-K} \frac{k}{K} z^K]. \quad (6)$$

One difference between the BGL and BCL parameterizations is the use of the threshold condition discussed in Appendix C. Here, BGL does not use the threshold condition while BCL does use it. The free parameters $a_{+,n}$ and $b_{+,n}$ are fitted by using least square fitting methods [31] and must satisfy the following unitarity conditions [27]

$$\sum_{n=0}^N |a_{+,n}|^2 \leq 1, \quad (7)$$

and [13, 28]

$$\sum_{j,k=0}^K B_{jk} b_{+,j} b_{+,k} \leq 1. \quad (8)$$

For $f_{+,BGL}$ we consider $N = 0, 1, 2$ and for $f_{+,BCL}$ we consider $K = 1, 2, 3$. It is important to note that N is not the number of parameters while K is, so to avoid confusion, the number of parameters used in the fit will be denoted n_p for both parameterizations, where $n_p = N + 1$ and $n_p = K$. The z^K term that is attached to every $b_{+,k}$ comes from the threshold condition which will be discussed in more detail in Appendix C.

The BGL parameterization sometimes includes a Blaschke factor $P_+(z)$ as well, which contains the information about the pole at $q_*^2 \equiv m_{B_c^*}^2 = 40.02 \text{ GeV}^2$. However, it has been shown that the Blaschke factor does not appreciably affect the z -fit for the BGL analysis of $B \rightarrow D \ell \nu_\ell$ due to the pole being very far away from the kinematical region [17]. For this reason the Blaschke factor has been set to 1 in [6, 17] and our definition in Eq. (4) follows this choice. While BCL replaces the commonly used outer function and Blaschke factor with a prefactor that has a pole at the same location as the Blaschke factor. The pole q_*^2 corresponds to $z(q_*^2, t_-) = -0.308$ and $z(q_*^2, t_{opt}) = -0.337$. The construction of the B_{jk} matrix can be found in [28], and we calculate the values B_{00} , B_{01} , B_{02} and B_{03} for $B \rightarrow D \ell \nu_\ell$ and display them in Table I. The remaining B_{mn} values can be calculated using the following

relations [28],

$$B_{j(j+k)} = B_{0k}, \quad (9)$$

and

$$B_{jk} = B_{kj}. \quad (10)$$

TABLE I. The matrix elements B_{jk} which are used in the BCL unitarity condition for $n_p = 1, 2, 3$.

B_{00}	B_{01}	B_{02}	B_{03}
0.0118	-0.0028	-0.0069	0.0038

The outer function and Blaschke factor are to some extent arbitrary so long that they are analytic and non-zero in the z range that we are interested in. Following [17] where they set the Blaschke factor equal to one, it is then interesting to investigate the parameterizations of Eqs. (4) and (6) with their prefactors set equal to one. To differentiate the form factors when there are no prefactors, we denote Eq. (4) with no prefactors as $f_{+,NN}$ and we denote Eq. (6) with no prefactors as $f_{+,NT}$, where NN stands for no-prefactor and no-threshold while NT stands for no-prefactor with-threshold. The explicit forms of $f_{+,NN}$ and $f_{+,NT}$ can be found below,

$$f_{+,NN}(z) = \sum_{n=0}^N a_{+,n} z^n, \quad (11)$$

and

$$f_{+,NT}(z) = \sum_{n=0}^{N-1} b_{+,n} [z^n - (-1)^{n-N} \frac{n}{N} z^N]. \quad (12)$$

Where NN uses $t_0 = t_-$ and NT uses $t_0 = t_{opt}$.

III. NEW METRICS AND RESULTS

We consider several tests that compare the goodness of fit and self-consistency of our models on the Belle data to determine the best parameterization with the best choices of

input parameters.

A. χ^2 Test

We use the LsqFit python library [31] to perform the fits of the different models with the Belle data, and the resulting fit parameters can be found in A. The LsqFit library also provides the χ^2 and reduced- χ^2 , χ_ν^2 , and these values are provided for BGL, BCL, NN and NT with 1p, 2p and 3p in Table II.

TABLE II. The χ^2 and χ_ν^2 values calculated from the fits performed on the differential decay width data with the BGL, BCL, NN and NT parameterizations with 1p, 2p and 3p.

	χ^2	χ_ν^2
BGL 1p	99	11
BGL 2p	4.56	0.57
BGL 3p	4.55	0.65
BCL 1p	33.3	3.7
BCL 2p	4.64	0.58
BCL 3p	4.55	0.65
NN 1p	135	15
NN 2p	4.88	0.61
NN 3p	4.55	0.65
NT 1p	135	15
NT 2p	5.04	0.63
NT 3p	4.55	0.65

It is clear that the 2p and 3p cases provide significantly better models than the 1p case due to the extremely high χ^2 and χ_ν^2 values in the 1p case. However it is not clear that the χ^2 provides significant discrimination between 2p and 3p for a given model or discrimination among the different models. Similar remarks apply to χ_ν^2 which increases by about 10% when going from 2p to 3p, which could be due to the data having ten bins. This leads us to needing another metric to be able to discriminate between the models.

B. Aikake Information Criterion

A test that enables quantitative comparisons between models with differing numbers of parameters that aren't rigorously possible without Bayesian techniques is the Aikake

Information Criterion (AIC). The AIC value is defined like an augmented χ^2 value, where the augment is adding a $2n_p$ term [32, 33],

$$\text{AIC} = 2n_p + \chi^2. \quad (13)$$

The inclusion of a penalty which is linear in n_p is used to discourage overfitting, and the factor 2 in front of n_p is discussed in [34]. Therefore, the preferred model will be the model that has the lowest AIC value. Changes in the AIC values ΔAIC when the number of degrees of freedom ν is changed by $\Delta\nu$ can be considered significant if $|\Delta\text{AIC}|/\text{AIC} > |\Delta\nu|/\nu$ [35].

These AIC values are displayed in Table III. The $2n_p$ term for 1p will not compensate for the drastically larger χ^2 value compared to the 2p and 3p fits, clearly showing that 1p is not descriptive enough. The AIC values in Table III show that all the 2p cases satisfy the inequality regarding ν , which indicates that the 2p case is preferred over the 3p case. However, the AIC values between BGL and BCL for the same number of parameters is still too close to determine anything significant about which of the models does a better job of fitting the Belle data. We proceed to define our own metrics to find one that is able to distinguish between the different parameterization options that we consider.

TABLE III. The AIC values calculated from the fits performed on the differential decay width data with the BGL, BCL, NN and NT parameterizations with 1p, 2p and 3p.

	AIC
BGL 1p	101
BGL 2p	8.56
BGL 3p	10.55
BCL 1p	35.3
BCL 2p	8.64
BCL 3p	10.55
NN 1p	137
NN 2p	8.88
NN 3p	10.55
NT 1p	137
NT 2p	9.04
NT 3p	10.55

C. Self-consistency metrics

In the form factor expressions, the polynomials in z are approximations of analytic functions in the kinematic range. The absence of singularities or cuts in that range implies that the exact knowledge of the function in an open region can uniquely determine the function in another region. This can be achieved by analytic continuation [29]. In the current context, if an analytic function is defined on an open segment of the real z axis corresponding to the kinematic range and if we partition this segment in a region \mathcal{H} corresponding to a high- z (or equivalently high- w or low- q^2) part and the complementary region \mathcal{L} in the low- z region. It is then clear that ideally the perfect knowledge of the function in \mathcal{H} , uniquely determines the function in \mathcal{L} and vice-versa.

In practice, if we use experimental data, we know the function at a finite number of points with a limited accuracy. It is expected that if we obtain a polynomial approximation in \mathcal{H} using the data in \mathcal{H} , that we call $f_+^{high}(z)$ and extend this polynomial to \mathcal{L} , and if we obtain $f_+^{low}(z)$ by swapping the roles of \mathcal{H} and \mathcal{L} , then the discrepancy

$$\Delta f(z) \equiv f_+^{high}(z) - f_+^{low}(z), \quad (14)$$

is nonzero and provide a measure of the inconsistency of the continuations due to imperfect knowledge of the function in addition to the uncertainty in the data.

A rough global measure of the inconsistency of a specific method used to obtain the polynomial approximation could be the L^2 -norm of $\Delta f(z)$. This quantity depends on the units of the form factor and the range of z in the integral. For a decent approximation, one would expect that $(\Delta f(z))^2$ would be of the order of the average experimental variance $\bar{\sigma}_{exp}^2$ and we could expect to get a quantity of order one by dividing by the length of the z -interval and the average experimental variance $\bar{\sigma}_{exp}^2 = 0.00199$. For these reasons we start with the dimensionless quantity

$$C_0 \equiv \frac{1}{\bar{\sigma}_{exp}^2 |z_{max} - z_{min}|} \int_{z_{min}}^{z_{max}} (\Delta f(z))^2 dz, \quad (15)$$

A more refined metric denoted C_1 , can be obtained by weighting *locally* with the inverse

local variance $\sigma_{exp}^2(z)$ obtained from the experimental data by interpolating with LsqFit.

$$C_1 \equiv \frac{1}{|z_{max} - z_{min}|} \int_{z_{min}}^{z_{max}} \frac{(\Delta f(z))^2}{\sigma_{exp}^2(z)} dz \quad (16)$$

When the experimental form factors are provided as binned data with n_b bins, we can define a discrete version of C_1 as

$$D_1 = \frac{1}{n_{bin}} \sum_{i=1}^{n_{bin}} \left(\frac{\Delta f_i}{\sigma_i} \right)^2, \quad (17)$$

with $\Delta f_i = \Delta f(z_i)$, z_i being in the middle of the i -th bin. This can be calculated in a straightforward way without the need of interpolations. If the bins are narrow enough, we expect that $D_1 \simeq C_1$. The general form of D_1 is reminiscent of a χ -square, however σ_i^2 is not the variance of Δf_i .

Given that the experimental binned data may involve significant correlations among the bins, we can pursue the analogy and generalize D_1 to

$$D_2 = \frac{1}{n_{bin}} \sum_{i,j=1}^{n_{bin}} \Delta f_i \mathcal{C}_{ij}^{-1} \Delta f_j, \quad (18)$$

with \mathcal{C}_{ij} the covariance matrix of the binned data for the form factor.

The covariance matrix \mathcal{C}_{ij} is calculated using sampled bootstrap form factor data points. Using the `gvar` python library [36], we generated $M = 10^4$ bootstrap differential decay width data sets generated from the Belle data using the underlying covariance matrix. Then using Eqs. (1) and (2), we converted the generated differential decay width data into data describing the form factor, with f^i being the set of random form factor data in the i -th bin. Finally, we calculated \mathcal{C}_{ij} using,

$$\mathcal{C}_{ij} = \frac{1}{M} \sum_{m=1}^M (f_m^i - \bar{f}^i)(f_m^j - \bar{f}^j) \quad (19)$$

Where f_m^i is the m -th data point in the i -th bin and \bar{f}^i is the mean of the data in the i -th bin. And the σ_i^2 from Eq. (19) is the diagonal entries of the covariance matrix, $\sigma_i^2 = \mathcal{C}_{ii}$.

The Belle data has $n_{bin} = 10$ bins, and we split the data in half between the \mathcal{L} and \mathcal{H} regions. We then fit the free parameters $a_{+,n}$ and $b_{+,n}$ to the \mathcal{L} region data and the \mathcal{H} region

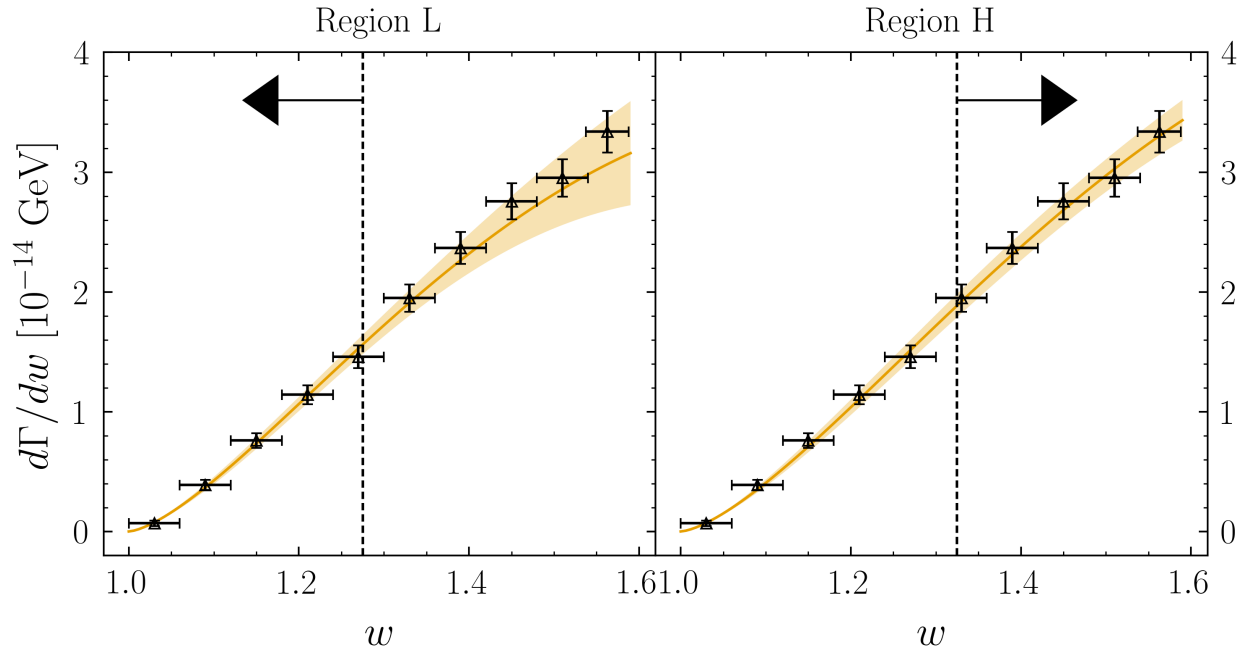


FIG. 1. The results of our fits using the BGL parameterization. The red line is the mean value of our fit and the lighter red region is the $1\text{-}\sigma$ error band, the black triangles are the Belle data with error bars, and the dashed arrow indicates whether region \mathcal{L} (left) or region \mathcal{H} (right) was used in the fit.

data separately. If we had perfect knowledge of f_+ in the \mathcal{L} region we could reconstruct it in the \mathcal{H} region and vice versa. An example of this is shown for BGL with 2p in Fig. 1 and for BCL with 2p in Fig. 2.

We carry out this method for BGL and BCL with 2p and 3p, and use the resulting parameters to plot the form factor $f_+(z)$ and convert the Belle data from differential decay width data to form factor data and include it in Figs. 3 and 4. Both BGL and BCL have more overlap between the fits for 2p than for 3p. In the 3p fits case, the error band is very small in the \mathcal{H} region and the error band increases in size as it moves into the \mathcal{L} region, but the \mathcal{L} fit has large error bands in both the \mathcal{L} and \mathcal{H} regions.

Now using the results of the fits for every parameterization with 1p, 2p and 3p, we are able to calculate the discrete and continuous metrics. The values of C_0 and C_1 that we calculate are listed in Table IV for all parameterizations with 1p, 2p and 3p, and D_1 and D_2 are similarly shown in Table V.

Since $\Delta f(z)$ reflects the discrepancy between fits and extrapolations, the most self-

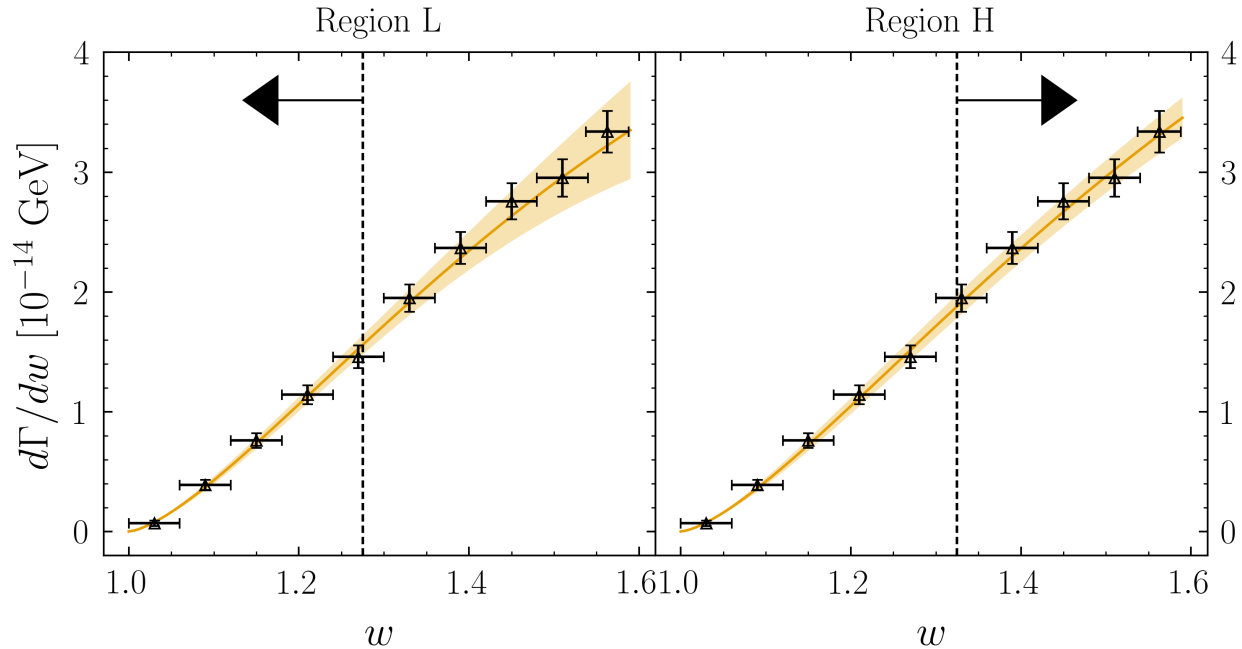


FIG. 2. Same as Fig. 1 but for the BCL parameterization.

TABLE IV. The C_0 and C_1 values for BGL, BCL, NN and NT with 1p, 2p and 3p.

	C_0	C_1
BGL 1p	15.76	39.44
BGL 2p	1.18	5.16
BGL 3p	17.56	91.76
BCL 1p	3.37	7.63
BCL 2p	0.63	2.72
BCL 3p	15.23	78.96
NN 1p	24.50	64.26
NN 2p	1.85	7.82
NN 3p	19.10	100.16
NT 1p	24.50	64.31
NT 2p	2.11	8.83
NT 3p	19.81	104.04

consistent model is the one with the lowest values of C_0 , C_1 , D_1 , and D_2 . We see that the 2p values are all considerably lower than the corresponding 1p or 3p values and are clearly preferred, which agrees with what we obtained with the AIC metrics. We define the mean values of the C_0 , C_1 , D_1 , and D_2 for only the 2p models as $\bar{C}_0^{2p} = 1.443$, $\bar{C}_1^{2p} = 6.133$, $\bar{D}_1^{2p} = 6.923$, and $\bar{D}_2^{2p} = 6.065$. Comparing the C_0 , C_1 and D_1 values from the 2p models

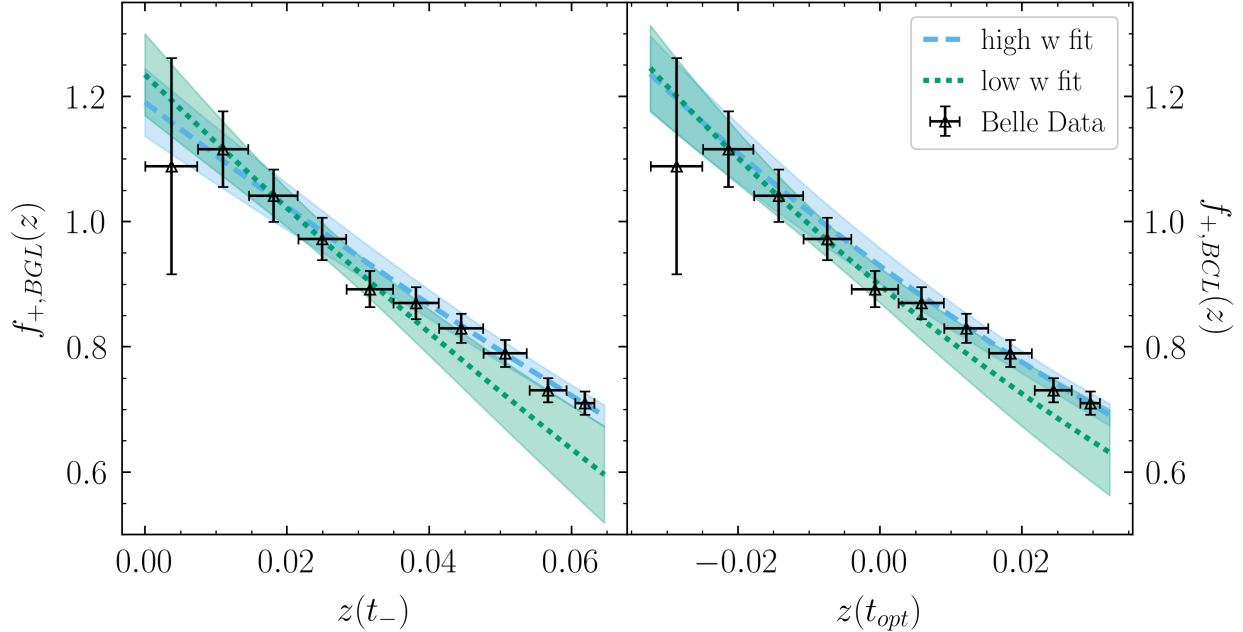


FIG. 3. Plots of the form factor $f_+(z)$ vs z using the results of our fits from regions \mathcal{L} and \mathcal{H} . The results of our BGL fit with 2p (Left), the results of our BCL fit with 2p (Right). The red dashed line and red band indicate the fit from region \mathcal{H} , and the blue dashed line and blue band indicate the fit from region \mathcal{L} .

TABLE V. The D_1 and D_2 values for BGL, BCL, NN and NT with 1p, 2p and 3p.

	D_1	D_2
BGL 1p	41.85	10.95
BGL 2p	5.78	4.76
BGL 3p	104.64	117.68
BCL 1p	8.02	1.90
BCL 2p	3.00	1.74
BCL 3p	89.85	100.37
NN 1p	68.54	19.02
NN 2p	8.88	8.21
NN 3p	115.43	126.79
NT 1p	68.54	19.02
NT 2p	10.03	9.55
NT 3p	119.70	131.76

with these mean values, the values from the BCL parameterization lie 55 – 56% below the mean values, the values from the BGL parameterization lie 15 – 18% below, the values from the NN parameterization lie 27 – 28% above the mean values, and the values from the NT

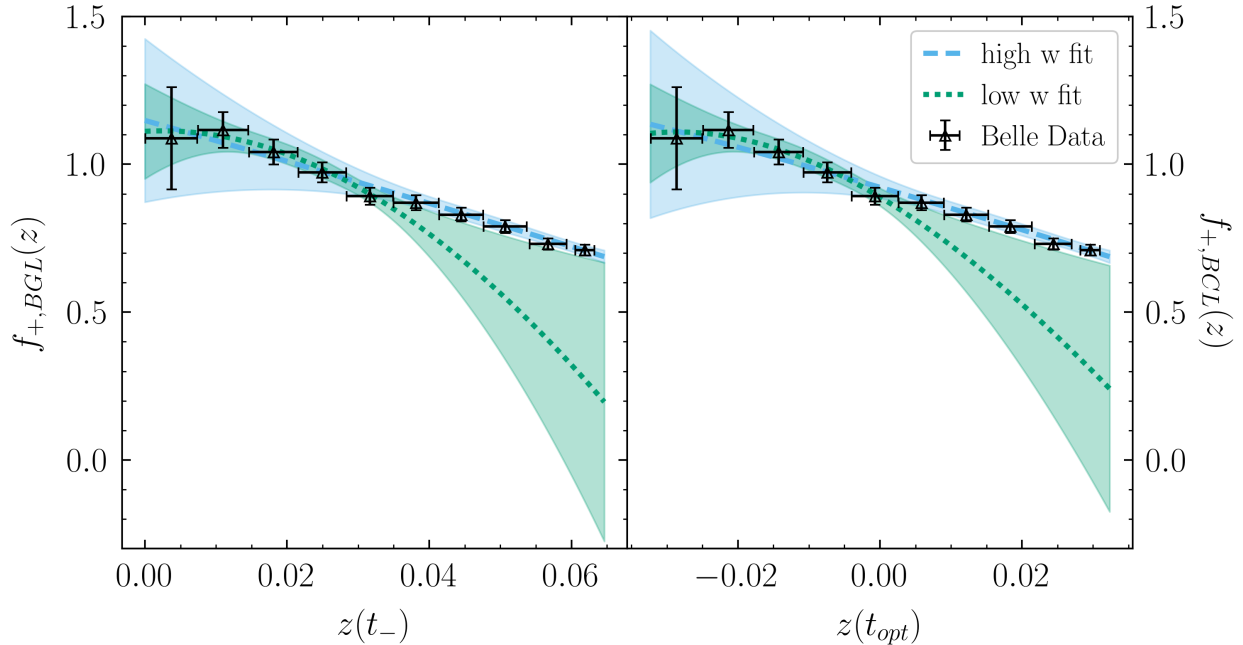


FIG. 4. Same as Fig. 3 but for 3p.

parameterization lie 43 – 46% above the mean values. For the D_2 values from the 2p models, BCL lies 71% below the mean value, BGL lies 21% below the mean value, NN lies 35% above the mean value and NT lies 57% above the mean value. For each metric with 2p compared to the mean values with 2p, the BCL parameterization is significantly lower than the mean and appears to be the most self-consistent from the point of view of analyticity.

We have also considered the effects of relaxing the threshold condition in BCL in C and changing the values of t_0 , namely using t_{opt} for BGL or t_- for BCL in B. The tables make clear that these choices affect the metrics by at most a few percents and are essentially irrelevant.

IV. ANALYSIS OF SELF-CONSISTENCY METRICS

In this section, we discuss the relations among the new metrics. First we will compare different metrics for a given parameterization and then we will compare the same metric but for different parameterizations.

A. Comparing the Metrics for a Given Parameterization

The first comparison that we make is between C_1 and C_0 . The ratios C_1/C_0 can be found in Table VI. The values in the 2p row are consistent within $\sim 3\%$ of each other, and the values in the 3p row are within $\lesssim 1\%$ of each other. In other words, the two metrics are proportional, with a proportionality constant which depends mostly on the number of parameters used in the fit. Note that the absolute normalization of C_0 or C_1 is not important. From the standard deviations in the binned data [6], we have

$$\frac{1}{n_{bin}} \sum_{i=1}^{n_{bin}} \frac{1}{\sigma_i^2} \simeq \frac{2.81}{\left(\frac{1}{n_{bin}} \sum_{i=1}^{n_{bin}} \sigma_i\right)^2}, \quad (20)$$

which partially explains that C_1 is larger than C_0 . We next look at D_1/C_1 . Since D_1 is a discrete version of C_1 , we expect relative differences of the order of $1/n_{bin} = 0.1$. We see that this is the case in Table VII.

TABLE VI. The ratio of C_1 to C_0 calculated with BGL, BCL, NN and NT for 2p and 3p.

	$C_{1,BGL}/C_{0,BGL}$	$C_{1,BCL}/C_{0,BCL}$	$C_{1,NN}/C_{0,NN}$	$C_{1,NT}/C_{0,NT}$
2p	4.373	4.318	4.227	4.185
3p	5.226	5.185	5.244	5.252

TABLE VII. The ratio of D_1 to C_1 calculated with BGL, BCL, NN and NT for 2p and 3p.

	$D_{1,BGL}/C_{1,BGL}$	$D_{1,BCL}/C_{1,BCL}$	$D_{1,NN}/C_{1,NN}$	$D_{1,NT}/C_{1,NT}$
2p	1.120	1.103	1.136	1.136
3p	1.140	1.138	1.154	1.151

In summary, we found that the three metrics C_0 , C_1 and D_1 provide consistent estimates of the departure from analyticity. For instance, we could just consider D_1 which is easier to calculate from experimental binned data. So far, we have ignored correlations among the bins. Table II of Ref. [6] shows that these correlations are significant which motivated the introduction of D_2 . The ratios D_2/D_1 are provided in Table VIII. We see that for 2p the ratios have a stronger dependence on the parameterization which amplifies the discrimination (a lower D_1 means an even lower D_2). On the other hand for the suboptimal choice 3p, the ratio is about 1.1 in the four cases and D_2 does not provide new information.

TABLE VIII. The ratio of D_2 to D_1 calculated with BGL, BCL, NN and NT for 2p and 3p.

	$D_{2,BGL}/D_{1,BGL}$	$D_{2,BCL}/D_{1,BCL}$	$D_{2,NN}/D_{1,NN}$	$D_{2,NT}/D_{1,NT}$
2p	0.824	0.580	0.925	0.952
3p	1.125	1.117	1.098	1.101

The values in the 3p row are consistent within $\lesssim 1\%$ of the other values in the 3p row, however we see that the D_2/D_1 ratio for 2p is smaller for BCL than it is for BGL, NN or NT by roughly 43%. It is great that these comparisons show consistency, and they show that the D_2 metric provides the most information to discriminate between the parameterizations.

B. Comparing the Same Metric for Different Parameterizations

Since the NN and NT parameterizations are not ever mentioned in the literature, at this point we ignore them and focus again on BGL and BCL as they were shown to be preferred over NN or NT by every metric we considered. Now comparing the same metric between the BGL and BCL parameterizations, the ratios $C_{i,BCL}/C_{i,BGL}$ for $i = 0, 1$ are given in Table IX and $D_{j,BCL}/D_{j,BGL}$ for $j = 1, 2$ in Table X. For this, we recalculated the BGL parameterization with $t_0 = t_{opt}$ and the BCL parameterization with $t_0 = t_-$, in order to have the z -expansion consistent when comparing different parameterizations.

TABLE IX. The ratio of $C_{i,BCL}$ to $C_{i,BGL}$ calculated for both 2p and 3p with both choices of t_0 .

	$C_{0,BCL}/C_{0,BGL}$		$C_{1,BCL}/C_{1,BGL}$	
	$t_0 = t_-$	$t_0 = t_{opt}$	$t_0 = t_-$	$t_0 = t_{opt}$
2p	0.536	0.545	0.523	0.532
3p	0.862	0.866	0.855	0.860

TABLE X. The ratio of $D_{j,BCL}$ to $D_{j,BGL}$ calculated for both 2p and 3p with both choices of t_0 .

	$D_{1,BCL}/D_{1,BGL}$		$D_{2,BCL}/D_{2,BGL}$	
	$t_0 = t_-$	$t_0 = t_{opt}$	$t_0 = t_-$	$t_0 = t_{opt}$
2p	0.515	0.524	0.360	0.370
3p	0.854	0.859	0.849	0.854

It is important to observe that the values in Tables IX and X for the 3p rows are all consistent within $\lesssim 1\%$ of the other values in the 3p rows. It is also important to see that the

values in the 2p rows are very similar for $C_{0,BCL}/C_{0,BGL}$, $C_{1,BCL}/C_{1,BGL}$ and $D_{1,BCL}/D_{1,BGL}$, however there is decrease of roughly 36% in the 2p values for $D_{2,BCL}/D_{2,BGL}$. This shows the consistency of our defined metrics, and shows that C_0 , C_1 and D_1 offer a similar amount of information compared to D_2 , which possibly contains more information about the fits because it is the only metric to differ in these categories when compared.

V. CONCLUSION

In conclusions, we investigated the BGL and BCL parameterizations of the form factor used in the differential decay rate of $B \rightarrow D\ell\nu_\ell$. With the experimental binned data collected by the Belle collaboration [6], we found that the standard χ^2 and χ_ν^2 do not provide us with enough information to distinguish between BGL vs BCL or 2p vs 3p. The AIC clearly favors 2p over 1p or 3p but the differences between BGL and BCL are too small to be meaningful.

We introduced four metrics or “cost functions” (C_0 , C_1 , D_1 and D_2) that measure the discrepancy between fits and extrapolations of the regular parts of form factors in the high and low parts of the kinematic range. Given the analyticity of these regular parts, a perfect fit in one region would provide a unique and perfect analytical continuation in the other region and vice-versa. The first metric (C_0) is a dimensionless L^2 norm of the discrepancy. C_1 is a locally weighted version of C_0 that favors the kinematic regions with smaller experimental uncertainties. D_1 is a discretized version of C_1 which can be implemented directly from the experimental binned data. D_2 is an extension of D_1 that incorporate the correlations among the bins. In view of the significant bin correlations [6], D_2 should be a better measure than D_1 . C_0 , C_1 , and D_1 provide very similar and consistent discriminations while D_2 somehow amplifies the discriminations for 2p.

All the metrics strongly favor 2p over 3p. A possible interpretation is that the experimental uncertainties prevent an accurate determination of the quadratic corrections and that one partially extrapolates the experimental noise which is not an analytical function of z . All the metrics favor 2p over 1p. Except for BCL, the metrics are about twice larger for 1p. It could be that the corrections to the constant approximation are significant and result in significantly different constant approximations in the high and low z regions. On the other hand, for BCL it appears that 1p is a better approximation than for the other

parameterization.

Focusing on the 2p results, we find a finer resolution among parameterizations. For all the metrics, we observe smaller values for BCL than for the other parameterizations. In addition BGL does better than no prefactor. It is possible that in the case considered here, the BCL prefactor captures the features of the actual form factor in a slightly better way. This is hinted by the fact that a constant approximation has a significantly smaller χ^2 for BCL. This observation may be anecdotal and study of other cases should bring more light on the question. We also found that other choices such as the the value of t_0 or the imposition of a threshold condition have a marginal impact on the values of the metrics.

It should be emphasized that all the metrics measure discrepancies among fits and not closeness to data. It might be possible to include them in augmented χ^2 [32, 33], however, determining the coefficient in front of the metric is a nontrivial task. It should also be noted that very recently, Bayesian inference methods have been used to deal with the truncation question [24] and applied to $B_s \rightarrow K\ell\nu_\ell$ [12]. These methods consider higher order expansions and provide results in agreement with other calculations based on unitarity [23]. It would be very interesting to repeat our analysis using this Bayesian inference procedure for the two sets of bins considered here separately and compare alternative higher-order expansions with our metrics.

So far our calculations of the metrics have been limited to one set of experimental data [6] for $B \rightarrow D\ell\nu_\ell$ and it is premature to draw general conclusions. Applying the method to other process involving the the z -expansion should help identifying more general properties. The z -expansion has also been used extensively in the study of nucleon form factors. Various neutrino-deuteron scattering experiments have been combined to extract the z -expansion of the isovector axial nucleon form factor from experiment [37]. The z -expansion has also been used to parameterize lattice calculations of the same quantity, see for instance [38–46] and more references in a recent review article [30]. These parameterizations have been used to incorporate nucleon effects in the calculations of neutrino-nucleus cross section [47]. The method that we proposed can be applied to nucleon form factors as long as one can perform new fits in distinct kinematic regions. This is feasible for binned data, but if extrapolations procedures are involved, such as the continuum limit in lattice calculations, all the details of the existing procedure need to be repeated in kinematic subregions.

ACKNOWLEDGMENTS

This research was supported in part by Department of Energy under Award Numbers DOE grant DE-SC0010113. We thank R. Van de Water for emphasizing the need of a metric involving covariances and for comments on the presentation. We thank M. Wagman for comments on the AIC criterion and for comments on the manuscript. We thank A. Kronfeld, and F. Herren for valuable discussions and A. Juttner and O. Witzel for pointing out recent references.

Appendix A: Our Calculated Fit Parameters

For completeness, we list the fit parameters that were the result of our fits to the Belle data. For 1p, 2p and 3p, we show the BGL and BCL fit parameters in [XI](#) and the NN and NT parameters in [XIII](#). We also provide the ratios of the fit parameters for BGL and BCL in [XII](#) and for NN and NT in [XIV](#).

TABLE XI. The $a_{+,n}$ and $b_{+,n}$ values that came from the global fit of BGL and BCL.

	BGL			BCL		
	$a_{+,0}$	$a_{+,1}$	$a_{+,2}$	$b_{+,0}$	$b_{+,1}$	$b_{+,2}$
1p	0.00804(19)	—	—	0.703(16)	—	—
2p	0.01238(41)	-0.0654(58)	—	0.773(19)	-2.41(42)	—
3p	0.01248(67)	-0.071(31)	0.07(37)	0.775(20)	-2.28(64)	-8(28)

TABLE XII. The ratios $a_{+,n+1}/a_{+,n}$ and $b_{+,n+1}/b_{+,n}$ using the central values of the parameters from [XI](#).

	BGL		BCL	
	$a_{+,1}/a_{+,0}$	$a_{+,2}/a_{+,1}$	$b_{+,1}/b_{+,0}$	$b_{+,2}/b_{+,1}$
2p	-5.281	—	-3.112	—
3p	-5.710	-0.99998	-2.942	3.716

Appendix B: Investigating the t_0 Parameter

The BGL and BCL parameterizations use different choices for t_0 , although the value of t_0 does not affect the size of the z range but it does affect the center of the z range. We

TABLE XIII. The $a_{+,n}$ and $b_{+,n}$ values that came from the global fit of NN and NT.

	NN			NT		
	$a_{+,0}$	$a_{+,1}$	$a_{+,2}$	$b_{+,0}$	$b_{+,1}$	$b_{+,2}$
1p	0.666(17)	—	—	0.666(17)	—	—
2p	1.154(37)	-7.22(53)	—	0.921(23)	-7.14(53)	—
3p	1.181(61)	-8.7(2.8)	18(33)	0.917(24)	-7.56(82)	18(32)

TABLE XIV. The ratios $a_{+,n+1}/a_{+,n}$ and $b_{+,n+1}/b_{+,n}$ using the central values of the parameters from [XIII](#).

	NN		NT	
	$a_{+,1}/a_{+,0}$	$a_{+,2}/a_{+,1}$	$b_{+,1}/b_{+,0}$	$b_{+,2}/b_{+,1}$
2p	-6.257	—	-7.750	—
3p	-7.404	-2.088	-8.236	-2.376

investigated the effect of t_0 on our metrics by calculating all the metrics using both choices of t_0 . The χ^2 , χ_ν^2 and AIC values can be found in [Table XV](#), and the C_0 , C_1 , D_1 and D_2 values can be found in [Table XVI](#).

TABLE XV. Same as [Tables II](#) and [III](#), but every value is calculated with both choices of t_0 .

	χ^2		χ_ν^2		AIC	
	$t_0 = t_-$	$t_0 = t_{opt}$	$t_0 = t_-$	$t_0 = t_{opt}$	$t_0 = t_-$	$t_0 = t_{opt}$
BGL 1p	99	99	11	11	101	101
BGL 2p	4.56	4.56	0.57	0.57	8.56	8.56
BGL 3p	4.55	4.55	0.65	0.65	10.55	10.55
BCL 1p	33.3	33.3	3.7	3.7	35.3	35.3
BCL 2p	4.64	4.64	0.58	0.58	8.64	8.64
BCL 3p	4.55	4.55	0.65	0.65	10.55	10.55
NN 1p	135	135	15	15	137	137
NN 2p	4.88	4.88	0.61	0.61	8.88	8.88
NN 3p	4.55	4.55	0.65	0.65	10.55	10.55
NT 1p	135	135	15	15	137	137
NT 2p	4.96	5.04	0.62	0.63	8.96	9.04
NT 3p	4.55	4.55	0.65	0.65	10.55	10.55

We find that the choice of t_0 has negligible effects on the χ^2 , χ_ν^2 and AIC metrics at all with the precision that we consider. However, the C_0 and C_1 as well as the D_1 and D_2 metrics have some minor differences based on the choice of t_0 , but the differences are on the order of 1%. This confirms that the main role of t_0 is to set the central value of the z range.

TABLE XVI. Same as Tables IV and V but every value is calculated with both choices of t_0 .

	C_0		C_1		D_1		D_2	
	$t_0 = t_-$	$t_0 = t_{opt}$	$t_0 = t_-$	$t_0 = t_{opt}$	$t_0 = t_-$	$t_0 = t_{opt}$	$t_0 = t_-$	$t_0 = t_{opt}$
BGL 1p	15.76	15.38	39.44	38.44	41.85	41.76	10.95	10.64
BGL 2p	1.18	1.16	5.16	5.11	5.78	5.72	4.76	4.69
BGL 3p	17.56	17.58	91.76	91.83	104.64	104.54	117.68	117.57
BCL 1p	3.37	3.37	7.62	7.63	8.02	8.02	1.90	1.90
BCL 2p	0.63	0.63	2.70	2.72	2.98	3.00	1.71	1.74
BCL 3p	15.13	15.23	78.44	78.96	89.39	89.85	99.85	100.37
NN 1p	24.50	24.50	64.26	64.26	68.54	68.54	19.02	19.02
NN 2p	1.85	1.87	7.82	7.88	8.88	8.95	8.21	8.29
NN 3p	19.10	19.19	100.16	100.66	115.43	115.81	126.79	127.23
NT 1p	24.50	24.50	64.31	64.31	68.54	68.54	19.02	19.02
NT 2p	2.09	2.11	8.72	8.83	9.92	10.03	9.42	9.55
NT 3p	19.69	19.81	103.42	104.04	119.70	119.70	131.16	131.76

Appendix C: BCL With No Threshold Condition

The threshold condition from [28] comes from $z(t_+, t_0) = -1$ which can be seen in Eq. (3), and from the fact that $(z + 1) \sim \text{const.} \times (q^2 - t_+)^{1/2}$ near $z = -1$. Then the threshold condition is,

$$\left[\frac{df_+}{dz} \right]_{z=-1} = 0. \quad (\text{C1})$$

We investigate the effect of the threshold condition by reproducing our results using the BCL parameterization with no threshold condition, which we call BCL* has the form,

$$f_{+,BCL^*}(z) = \frac{1}{1 - q^2(z)/m_{B_c^*}^2} \sum_{n=0}^N b_{+,n} z^n. \quad (\text{C2})$$

Using this BCL*, we recalculate all the values in Tables XV and XVI and display the results below.

TABLE XVII. Same as Table XV but using BCL*.

	χ^2		χ_ν^2		AIC	
	$t_0 = t_-$	$t_0 = t_{opt}$	$t_0 = t_-$	$t_0 = t_{opt}$	$t_0 = t_-$	$t_0 = t_{opt}$
BCL* 1p	33.3	33.3	3.7	3.7	35.3	35.3
BCL* 2p	4.64	4.64	0.58	0.58	8.64	8.64
BCL* 3p	4.55	4.55	0.65	0.65	10.55	10.55

TABLE XVIII. Same as Table XVI but using BCL*.

	C_0		C_1		D_1		D_2	
	$t_0 = t_-$	$t_0 = t_{opt}$	$t_0 = t_-$	$t_0 = t_{opt}$	$t_0 = t_-$	$t_0 = t_{opt}$	$t_0 = t_-$	$t_0 = t_{opt}$
BCL* 1p	3.37	3.37	7.62	7.63	8.04	8.04	1.93	1.93
BCL* 2p	0.63	0.61	2.65	2.55	2.96	2.84	1.61	1.54
BCL* 3p	17.03	17.88	88.14	77.00	102.68	89.58	109.22	96.28

These values are mostly identical to the BCL values shown in Tables XV and XVI, with the only differences appearing in C_0 , C_1 , D_1 and D_2 .

-
- [1] Bernard Aubert *et al.* (BaBar), “Determination of the form-factors for the decay $B^0 \rightarrow D^{*-}\ell^+\nu_\ell$ and of the CKM matrix element $|V_{cb}|$,” *Phys. Rev. D* **77**, 032002 (2008), [arXiv:0705.4008 \[hep-ex\]](#).
 - [2] Bernard Aubert *et al.* (BaBar), “A Measurement of the branching fractions of exclusive $\bar{B} \rightarrow D^{(*)}(\pi)\ell^-\bar{\nu}(\ell)$ decays in events with a fully reconstructed B meson,” *Phys. Rev. Lett.* **100**, 151802 (2008), [arXiv:0712.3503 \[hep-ex\]](#).
 - [3] P. del Amo Sanchez *et al.* (BaBar), “Study of $B \rightarrow \pi\ell\nu$ and $B \rightarrow \rho\ell\nu$ Decays and Determination of $|V_{ub}|$,” *Phys. Rev. D* **83**, 032007 (2011), [arXiv:1005.3288 \[hep-ex\]](#).
 - [4] J. P. Lees *et al.* (BaBar), “Branching fraction and form-factor shape measurements of exclusive charmless semileptonic B decays, and determination of $|V_{ub}|$,” *Phys. Rev. D* **86**, 092004 (2012), [arXiv:1208.1253 \[hep-ex\]](#).
 - [5] H. Ha *et al.* (Belle), “Measurement of the decay $B^0 \rightarrow \pi^-\ell^+\nu$ and determination of $|V_{ub}|$,” *Phys. Rev. D* **83**, 071101 (2011), [arXiv:1012.0090 \[hep-ex\]](#).
 - [6] R. Glattauer and et. al, *Phys. Rev. D* **93**, 032006 (2016), [arXiv:1510.03657v3 \[hep-ex\]](#).
 - [7] E. Waheed *et al.* (Belle), “Measurement of the CKM matrix element $|V_{cb}|$ from $B^0 \rightarrow D^{*-}\ell^+\nu_\ell$ at Belle,” *Phys. Rev. D* **100**, 052007 (2019), [Erratum: *Phys.Rev.D* **103**, 079901 (2021)], [arXiv:1809.03290 \[hep-ex\]](#).
 - [8] F. Abudinén *et al.* (Belle-II), “Measurement of the semileptonic $\bar{B}^0 \rightarrow D^{*+}\ell^-\nu_\ell$ branching fraction with fully reconstructed B meson decays and 34.6 fb⁻¹ of Belle II data,” (2020), [arXiv:2008.10299 \[hep-ex\]](#).

- [9] F. Abudinén *et al.* (Belle-II), “Studies of the semileptonic $\bar{B}^0 \rightarrow D^{*+} \ell^- \bar{\nu}_\ell$ and $B^- \rightarrow D^0 \ell^- \bar{\nu}_\ell$ decay processes with 34.6 fb^{-1} of Belle II data,” (2020) [arXiv:2008.07198 \[hep-ex\]](#).
- [10] Jon A. Bailey *et al.*, “The $B \rightarrow \pi \ell \nu$ semileptonic form factor from three-flavor lattice QCD: A Model-independent determination of $|V_{ub}|$,” *Phys. Rev. D* **79**, 054507 (2009), [arXiv:0811.3640 \[hep-lat\]](#).
- [11] C. Bernard *et al.*, “Visualization of semileptonic form factors from lattice QCD,” *Phys. Rev. D* **80**, 034026 (2009), [arXiv:0906.2498 \[hep-lat\]](#).
- [12] Jonathan M. Flynn, Ryan C. Hill, Andreas Jüttner, Amarjit Soni, J. Tobias Tsang, and Oliver Witzel, “Exclusive semileptonic $B_s \rightarrow K \ell \nu$ decays on the lattice,” (2023), [arXiv:2303.11280 \[hep-lat\]](#).
- [13] Jon A. Bailey *et al.* (Fermilab Lattice, MILC), “ $|V_{ub}|$ from $B \rightarrow \pi \ell \nu$ decays and (2+1)-flavor lattice QCD,” *Phys. Rev. D* **92**, 014024 (2015), [arXiv:1503.07839 \[hep-lat\]](#).
- [14] Jon A. Bailey *et al.* (Fermilab Lattice, MILC), “ $B \rightarrow \pi \ell \ell$ form factors for new-physics searches from lattice QCD,” *Phys. Rev. Lett.* **115**, 152002 (2015), [arXiv:1507.01618 \[hep-ph\]](#).
- [15] Heechang Na, Chris M. Bouchard, G. Peter Lepage, Chris Monahan, and Junko Shigemitsu, “ $B \rightarrow D \ell \nu$ form factors at nonzero recoil and extraction of $|V_{cb}|$,” *Physical Review D* **92** (2015), [10.1103/physrevd.92.054510](#).
- [16] Jon A. Bailey *et al.*, “ $B \rightarrow K l^+ l^-$ Decay Form Factors from Three-Flavor Lattice QCD,” *Phys. Rev. D* **93**, 025026 (2016), [arXiv:1509.06235 \[hep-lat\]](#).
- [17] Jon A. Bailey *et al.* (MILC), “ $B \rightarrow D \ell \nu$ form factors at nonzero recoil and $|V_{cb}|$ from 2+1-flavor lattice QCD,” *Phys. Rev. D* **92**, 034506 (2015), [arXiv:1503.07237 \[hep-lat\]](#).
- [18] Z. Gelzer *et al.* (Fermilab Lattice, MILC), “ B -meson semileptonic form factors on (2+1+1)-flavor HISQ ensembles,” *PoS LATTICE2019*, 236 (2019), [arXiv:1912.13358 \[hep-lat\]](#).
- [19] A. Bazavov *et al.* (Fermilab Lattice, MILC, Fermilab Lattice, MILC), “Semileptonic form factors for $B \rightarrow D^* \ell \nu$ at nonzero recoil from 2 + 1-flavor lattice QCD: Fermilab Lattice and MILC Collaborations,” *Eur. Phys. J. C* **82**, 1141 (2022), [Erratum: *Eur.Phys.J.C* **83**, 21 (2023)], [arXiv:2105.14019 \[hep-lat\]](#).
- [20] W. G. Parrott, C. Bouchard, C. T. H. Davies, and D. Hatton, “Toward accurate form factors for B -to-light meson decay from lattice QCD,” *Phys. Rev. D* **103**, 094506 (2021), [arXiv:2010.07980 \[hep-lat\]](#).

- [21] W. G. Parrott, C. Bouchard, and C. T. H. Davies (HPQCD collaboration), “ $B \rightarrow K$ and $D \rightarrow K$ form factors from fully relativistic lattice QCD,” *Phys. Rev. D* **107**, 014510 (2023).
- [22] Laurence J. Cooper, Christine T. H. Davies, and Matthew Wingate (HPQCD), “Form factors for the processes $B_c^+ \rightarrow D^0 \ell^+ \nu_\ell$ and $B_c^+ \rightarrow D_s^+ \ell^+ \ell^+ (\nu \bar{\nu})$ from lattice QCD,” *Phys. Rev. D* **105**, 014503 (2022), [arXiv:2108.11242 \[hep-lat\]](#).
- [23] M. Di Carlo, G. Martinelli, M. Naviglio, F. Sanfilippo, S. Simula, and L. Vittorio, “Unitarity bounds for semileptonic decays in lattice QCD,” *Physical Review D* **104** (2021), [10.1103/physrevd.104.054502](#).
- [24] J. M. Flynn, A. Jüttner, and J. T. Tsang, “Bayesian inference for form-factor fits regulated by unitarity and analyticity,” (2023), [arXiv:2303.11285 \[hep-ph\]](#).
- [25] Susumu Okubo, “New improved bounds for K_{l3} parameters,” *Phys. Rev. D* **4**, 725–733 (1971).
- [26] Susumu Okubo, “Exact bounds for K_{l3} decay parameters,” *Phys. Rev. D* **3**, 2807–2813 (1971).
- [27] C. G. Boyd, B. Grinstein, and R. F. Lebed, *Phys.Rev.Lett.*74:4603-4606 (1995), [arXiv:9412324v3 \[hep-th\]](#).
- [28] Claude Bourrely, Laurent Lellouch, and Irinel Caprini, “Model-independent description of $B \rightarrow \pi l \nu$ decays and a determination of $|V_{ub}|$,” *Phys. Rev. D* **79**, 013008 (2009).
- [29] K. Knopp, *Theory of Functions, Parts I and II*, Dover Books on Mathematics (Dover Publications, 2013).
- [30] Aaron S. Meyer, André Walker-Loud, and Callum Wilkinson, “Status of Lattice QCD Determination of Nucleon Form Factors and their Relevance for the Few-GeV Neutrino Program,” (2022), [10.1146/annurev-nucl-010622-120608](#), [arXiv:2201.01839 \[hep-lat\]](#).
- [31] Peter Lepage and Christoph Gohlke, “[gplepage/lqfit: lqfit version 13.0](#),” (2022).
- [32] William I. Jay and Ethan T. Neil, “Bayesian model averaging for analysis of lattice field theory results,” *Phys. Rev. D* **103**, 114502 (2021).
- [33] E. T. Neil and J. W. Sitison, “Improved information criteria for bayesian model averaging in lattice field theory,” (2022), [10.48550/arXiv.2208.14983](#), [arXiv:2208.14983 \[hep-lat\]](#).
- [34] Hirotugu Akaike, “A new look at the statistical model identification,” *IEEE Transactions on Automatic Control* **19**, 716–723 (1974).
- [35] S. R. Beane *et al.* (NPLQCD, QCDSF), “Charged multihadron systems in lattice QCD+QED,” *Phys. Rev. D* **103**, 054504 (2021), [arXiv:2003.12130 \[hep-lat\]](#).

- [36] Peter Lepage, Christoph Gohlke, and Daniel Hackett, “[gplepage/gvar: gvar version 11.11.2](#),” (2023).
- [37] Aaron S. Meyer, Minerba Betancourt, Richard Gran, and Richard J. Hill, “Deuterium target data for precision neutrino-nucleus cross sections,” *Phys. Rev. D* **93**, 113015 (2016), [arXiv:1603.03048 \[hep-ph\]](#).
- [38] Ken-Ichi Ishikawa, Yoshinobu Kuramashi, Shoichi Sasaki, Natsuki Tsukamoto, Akira Ukawa, and Takeshi Yamazaki (PACS), “Nucleon form factors on a large volume lattice near the physical point in 2+1 flavor QCD,” *Phys. Rev. D* **98**, 074510 (2018), [arXiv:1807.03974 \[hep-lat\]](#).
- [39] Andreas S. Kronfeld, David G. Richards, William Detmold, Rajan Gupta, Huey-Wen Lin, Keh-Fei Liu, Aaron S. Meyer, Raza Sufian, and Sergey Syritsyn (USQCD), “Lattice QCD and Neutrino-Nucleus Scattering,” *Eur. Phys. J. A* **55**, 196 (2019), [arXiv:1904.09931 \[hep-lat\]](#).
- [40] Yong-Chull Jang, Rajan Gupta, Boram Yoon, and Tanmoy Bhattacharya, “Axial Vector Form Factors from Lattice QCD that Satisfy the PCAC Relation,” *Phys. Rev. Lett.* **124**, 072002 (2020), [arXiv:1905.06470 \[hep-lat\]](#).
- [41] Yong-Chull Jang, Rajan Gupta, Huey-Wen Lin, Boram Yoon, and Tanmoy Bhattacharya, “Nucleon electromagnetic form factors in the continuum limit from (2+1+1)-flavor lattice QCD,” *Phys. Rev. D* **101**, 014507 (2020), [arXiv:1906.07217 \[hep-lat\]](#).
- [42] Gunnar S. Bali, Lorenzo Barca, Sara Collins, Michael Gruber, Marius Löffler, Andreas Schäfer, Wolfgang Söldner, Philipp Wein, Simon Weishäupl, and Thomas Wurm (RQCD), “Nucleon axial structure from lattice QCD,” *JHEP* **05**, 126 (2020), [arXiv:1911.13150 \[hep-lat\]](#).
- [43] C. Alexandrou *et al.*, “Nucleon axial and pseudoscalar form factors from lattice QCD at the physical point,” *Phys. Rev. D* **103**, 034509 (2021), [arXiv:2011.13342 \[hep-lat\]](#).
- [44] Sungwoo Park, Rajan Gupta, Boram Yoon, Santanu Mondal, Tanmoy Bhattacharya, Yong-Chull Jang, Bálint Joó, and Frank Winter (Nucleon Matrix Elements (NME)), “Precision nucleon charges and form factors using (2+1)-flavor lattice QCD,” *Phys. Rev. D* **105**, 054505 (2022), [arXiv:2103.05599 \[hep-lat\]](#).
- [45] L. Alvarez Ruso *et al.*, “Theoretical tools for neutrino scattering: interplay between lattice QCD, EFTs, nuclear physics, phenomenology, and neutrino event generators,” (2022), [arXiv:2203.09030 \[hep-ph\]](#).

- [46] Dalibor Djukanovic, Georg von Hippel, Jonna Koponen, Harvey B. Meyer, Konstantin Ottnad, Tobias Schulz, and Hartmut Wittig, “Isovector axial form factor of the nucleon from lattice QCD,” *Phys. Rev. D* **106**, 074503 (2022), [arXiv:2207.03440 \[hep-lat\]](#).
- [47] Daniel Simons, Noah Steinberg, Alessandro Lovato, Yannick Meurice, Noemi Rocco, and Michael Wagman, “Form factor and model dependence in neutrino-nucleus cross section predictions,” (2022), [arXiv:2210.02455 \[hep-ph\]](#).